arXiv:1606.04499v2 [cond-mat.soft] 30 Sep 2016

Age and Structure of a Model Vapor-Deposited Glass

Daniel R. Reid*[1], Ivan Lyubimov†[1], M. D. Ediger‡[2], and Juan J. de Pablo§[1,3]

[1]Institute for Molecular Engineering, University of Chicago, 5640 South Ellis Avenue Chicago, Illinois 60637
[2]Department of Chemistry, University of Wisconsin - Madison, Madison, WI 53706
[3]Argonne National Laboratory, Argonne, IL

*danielreid@uchicago.edu
†ilyubimo@uchicago.edu
‡ediger@chem.wisc.edu
§depablo@uchicago.edu; Corresponding author

Abstract

Glass films prepared by a process of physical vapor deposition have been shown to have thermodynamic and kinetic stability comparable to those of ordinary glasses aged for thousands of years. A central question in the study of vapor-deposited glasses, particularly in light of new knowledge regarding anisotropy in these materials, is whether the ultra-stable glassy films formed by vapor deposition are ever equivalent to those obtained by liquid cooling. We present a computational study of vapor deposition for a two-dimensional glass forming liquid using a methodology which closely mimics experiment. We find that for the model considered here, structures that arise in vapor-deposited materials are statistically identical to those observed in ordinary glasses, provided the two are compared at the same inherent structure energy. We also find that newly deposited hot molecules produce cascades of hot particles that propagate far into the film, possibly influencing the relaxation of the material.

Introduction

Glasses represent kinetically arrested states of matter, whose characteristics depend strongly on the process of formation[1]. They are generally prepared by gradual cooling of a liquid to temperatures below the glass transition, T_g, of the corresponding bulk material. The properties of liquid-cooled, "ordinary" glasses depend on cooling rate and on the "age" of the glass - the amount of time that the material is allowed to rest at a given temperature (below T_g). Lower cooling rates (or ageing) lead to materials that lie deeper in the underlying potential energy landscape. They tend to have a higher density[2, 3], greater mechanical strength[4], lower enthalpy[2] and higher onset temperature (the temperature at which the film transforms from a glass into a liquid upon heating)[5], than those prepared by fast cooling. Higher stability is desirable in a wide range of applications, from organic electronics[6] to drug delivery[7].

Recent experimental work has shown that glasses prepared by a process of physical vapor deposition (PVD) can reach levels of stability that are equivalent to those of liquid-cooled glasses allowed to age for thousands of years[3, 8]. These highly stable PVD glasses are formed by depositing the glass former onto a substrate whose temperature is somewhat lower than T_g. It has been proposed that newly deposited molecules can freely explore configurational space near the surface of the growing film[9, 10], leading to molecular arrangements that correspond to lower free energy states than those accessible by quenching a bulk liquid [3].

The properties of three-dimensional (3D) PVD glasses have also been examined in computer simulations. On the one hand, results for a 3D model glass former consisting of a binary mixture of spherical particles indicate that vapor deposition leads to materials that exhibit higher kinetic stability, and whose structure is similar to that of their liquid-cooled counterparts[11]. On the other hand, simulations of model glasses consisting of anisotropic molecules suggest that a PVD process leads to materials that exhibit varying amounts of anisotropy[12]. Importantly, past simulations of vapor deposited glasses have relied on a formation process that involves repeated minimizations of potential energy, which are introduced for computational reasons. As such, past studies have been unable to reveal the role that hot molecules impacting a surface can have on the relaxation of the underlying glassy film. A recent study investigated the formation of highly stable 2D glasses prepared through a "pinning" technique[13]. The authors formed equilibrium glasses by freezing in-place a small fraction of the particles in a glass-forming liquid, raising the glass transition temperature above the current temperature, and glassifying the system in an equilibrium configuration. As insightful as the results from the pinning strategy have been, however, such glasses do not incorporate the presence of an interface into the simulations.

Past studies of two-dimensional (2D) systems have shed considerable light into the behavior of glasses. A variety of colloidal particles, including polystyrene and latex, have been shown to assemble into monolayers exhibiting varying degrees of local and long-range order [14, 15]. By virtue of being quasi-2D, such studies allow for the direct observation of glassy dynamics, including structural relaxation near the glass transition, thereby serving as a source of validation for theory and simulations [16, 17]. Atomic 2D glasses have also been prepared, consisting of silica on a graphene substrate [18, 19]. Such systems show a coexistence between crystalline and amorphous regions, which range in size from several unit cells to tens of nanometers across. Going beyond systems of spherical particles, 2D colloidal glasses have been formed using ellipsoids in order resist crystallization [20].

In this work we build upon these past studies by introducing a PVD formation approach that mimics closely that employed in experiments. Specifically, we avoid the artificial energy minimizations and temperature controls that were employed in past computational studies of 3D systems. Furthermore, by restricting our simulations to 2D systems, where configurations can be more easily visualized and inspected, we arrive at unambiguous correlations between local structure and energetic stability. Three important results emerge from our analysis. First, in contrast to previous reports, we find that vapor deposition leads to glasses whose energetic stability far exceeds that of samples prepared by liquid cooling. Second, it is shown that newly deposited particles generate cascades of hot particles that could serve to relax the interior of the film, and that help explain the advantages of PVD processes for preparation of new glasses. Third, we find that the structure of PVD glasses is isotropic and identical to that of liquid-cooled glasses, provided these two classes of materials are compared under preparation conditions for which their inherent structure energies are comparable.

Results

Model system

The details of the vapor deposition simulations presented here are discussed in the Methods section. Here we point out that the model considered in this study consists of a binary mixture of spheres whose glass-forming behavior in the bulk has been examined exhaustively, and that vapor-deposited samples are prepared by depositing groups of hot vapor particles onto a substrate held at a temperature T_s. Particles are deposited until a desired film thickness of approximately 35 molecular diameters is reached. Liquid-cooled samples are prepared by heating vapor deposited films above T_g, and then cooling them at a constant rate to a temperature near zero. A representative system is shown in Figure 1, where the blue layer at the bottom represents the substrate, the white spheres are of type A, and the black spheres are of type B. Additional sample films are shown in Figures 1 and 2 of Supplementary Information. Vapor-deposited and liquid-cooled films are prepared using a wide range of deposition and cooling rates. The inherent structure energy E_{IS} of a configuration, used to quantify its stability, is the potential energy of a configuration brought to its local energy minimum.

The 2D model considered here exhibits considerable local structure; to quantify this structure, we rely on two bond order parameters that assign values to each particle based on the configuration of its neighbors [21]. The first, denoted by q_5, selects for local pentagonal order. The second, q_8, selects for local rectangular order. The background colors in Figure 1 correspond to the magnitude of such order parameters.

Energetic properties

The energetic properties of PVD glasses are determined using only particles in the "bulk" region of the films, which is highlighted in Figure 2. It corresponds to a wide domain of constant density and composition. Figure 2 shows results for a variety of PVD and liquid-cooled films. From Figure 2, we point out two features that arise at the surface of these films: first, the density near the surface decreases gradually. This results from the surface being uneven, as density is simply taken as the number density at a horizontal cross section. Second, χ_A, the mole fraction of type A, rises near the surface of the films, as shown by previously Shi et al.[22]. More stable configurations maximize A-B interactions, as ϵ_{AB} is larger than ϵ_{AA} and ϵ_{BB}. Type A particles, which are more abundant at $\chi_A = 65\%$, segregate to the surface to maximize these interactions.

The inherent structure energy, E_{IS}, is an effective measure of the position of a glass on the potential energy landscape [23]. Inherent structure energies of several liquid-cooled and PVD films are shown in Panel (a) of Figure 3. The deposition time for vapor deposited films, t_{dep}, corresponds to the interval between addition of new groups of particles to the growing film. During this time, newly deposited particles are allowed to cool down and become integrated into the growing film. The cooling time, t_{cool}, is the time over which an ordinary film is cooled from $T = 5\,T_g$ to $T = 0.2\,T_g$. Cooling and deposition times are expressed in units of the alpha relaxation time of this system, τ_α, which is calculated using the self-intermediate scattering function at $T = 1.10\,T_g$ (Supplementary Fig. 3). For all simulations, new,

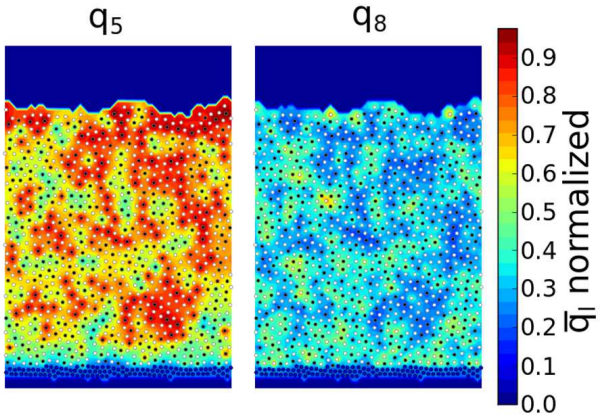

Figure 1: Diagram of liquid-cooled sample formed with $t_{cool} = 1.4 \times 10^1 \tau_\alpha$. Type A and B atoms are shown in white and black, respectively, while substrate atoms are shown in blue. This film has an inherent structural energy, E_{IS}, of -3.90. The background coloring in the left and right panels represents values of bond order parameters q_5 and q_8 as discussed in the Structural features section. Substrate atoms are held tightly in place once equilibrated using harmonic springs. Atoms are kept inside the simulation box using a harmonic repulsive wall as described in Methods.

"hot" particles are introduced into the system with an initial temperature of $T_i = 5.0\,T_g$. The simulated bulk T_g for this material is approximately 0.21 in Lennard-Jones units, as determined by taking the fictive temperature of a liquid-cooled film prepared with $t_{cool} = 1.4 \times 10^3\,\tau_\alpha$.

Previous experimental work has shown that the optimal substrate temperature, T_s, for the formation of glasses via PVD lies in the vicinity of $0.85\,T_g$[3, 8, 24, 25]. For the 2D model system considered here, we find that that the optimal substrate temperature (that leading to the lowest inherent structure energy) for a given deposition time decreases as deposition slows. PVD samples formed with $t_{dep} = 1.4 \times 10^0$ show an optimal T_s of $0.87\,T_g$, while samples formed with $t_{dep} = 1.4 \times 10^4 \tau_\alpha$ show an optimal T_s of $0.68\,T_g$ of T_g (Supplementary Table 1). Furthermore, PVD samples prepared at lower deposition rates exhibit significantly lower inherent-structure energies than those prepared at faster rates. As can be appreciated in Figure 3, depositing with $t_{dep} = 1.4 \times 10^4\,\tau_\alpha$ and $T_s = 0.68\,T_g$ gives $E_{IS} = -3.965$ while $t_{dep} = 1.4 \times 10^0\,\tau_\alpha$ and $T_s = 0.87\,T_g$ gives $E_{IS} = -3.918$. Optimal temperatures are found by fitting a cubic spline to the values of E_{IS} vs. T_s in panel (a) Figure 3 and taking the temperature at the minimum energy value.

We suggest that the ideal deposition temperature decreases with slower deposition rate due to a competition between thermodynamics and kinetics. As the substrate temperature decreases, lower energy states become more thermodynamically favorable, but the kinetics to reach such states become slower. As films are formed through more gradual deposition, atoms are allowed more time to approach equilibrium energy states. As originally proposed by Swallen et al., the ideal substrate temperature is where an ideal trade-off is found between which states the system is moving towards (thermodynamics) and how closely the system can approach those states (kinetics)[3].

Panel (b) in Figure 3 shows E_{IS} of liquid-cooled films evaluated at $T = 0.25\,T_g$ as a function of cooling time (t_{cool}). Previous work on 3D models suggests that E_{IS} varies linearly with $\log(t_{cool})$ [26, 11]. The 2D glass model considered here exhibits a nonlinear dependence. As shown in Panel (b) of Figure 3, a power-law fit of the form:

$$E_{IS} = 0.090\,t_{cool}^{-0.087} - 3.98 \tag{1}$$

describes our results reasonably well. Equation 1 can be used to estimate how slowly a liquid should be cooled to form ordinary glass films having inherent structure energies comparable to those of PVD films. These estimated cooling rates are shown by crosses in panel (b) of Figure 3, for t_{dep} values ranging from 1.4×10^0 to 1.4×10^4, separated by order-of-magnitude intervals. On the basis of this simple extrapolation, one can anticipate the most stable PVD configuration prepared here to be equivalent to a liquid-cooled sample prepared with $t_{cool} = 1.6 \times 10^{10} \tau_\alpha$, which is 1.1×10^5 times longer than the time utilized for the slowest cooling rate that we could accomplish with our computational resources.

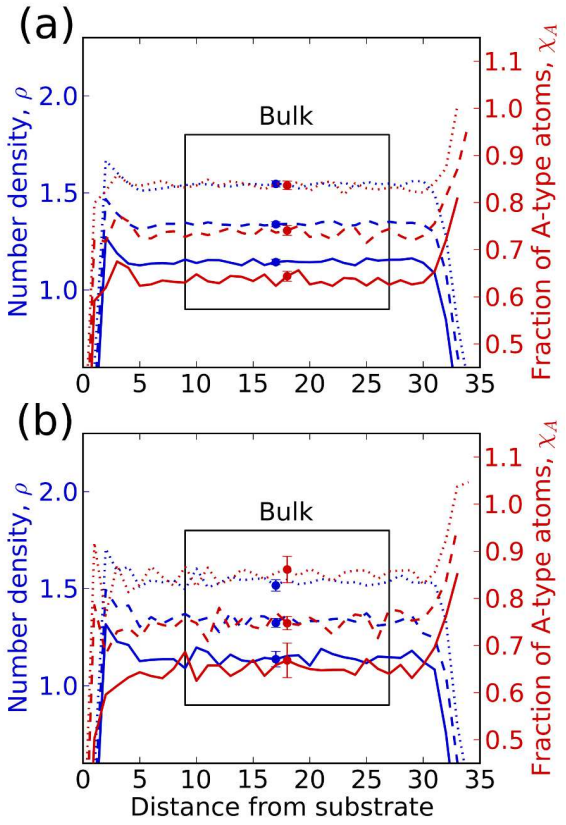

Figure 2: Number density and composition for liquid-cooled and vapor deposited films formed under several conditions. Data for liquid-cooled films are shown in Panel (a) while data for vapor deposited films are shown in Panel (b). The dotted, dashed, and solid lines represent films formed with $t = 1.4 \times 10^{(1,2,3)}$ at film temperatures of (0.75, 0.85, 0.85) T_g. From top to bottom in each figure, ρ is offset by (0.4, 0.2, 0.0) and χ_A is offset by (0.2, 0.1, 0.0). In (a), t refers to t_{cool} and T refers to the film's current temperature in the course of cooling. In (b), t refers to t_{dep} and T refers to substrate temperature. Only atoms in the bulk region shown are used in calculations unless otherwise specified. We define the bulk region to be several σ_{AA} away from where bulk composition and density properties are reached to ensure that edge effects are not present in the data. Error bars represent 95% confidence intervals.

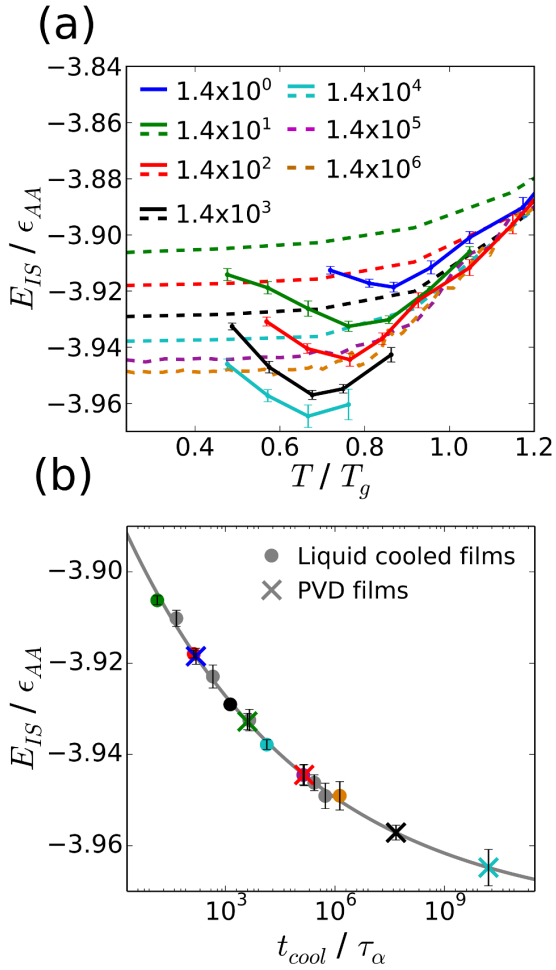

Figure 3: Inherent structure energy of PVD and liquid-cooled films along with predicted liquid-cooling rates required to form films with energy equal to that of PVD films. (a) Inherent structure energy of PVD and liquid-cooled films vs. temperature. Dashed lines represent liquid-cooled data while solid lines represent PVD data. For liquid-cooled samples, the film's temperature refers to the temperature at which E_{IS} was calculated during its linear cooling. For PVD films, temperature refers to the substrate temperature with which the film was formed. Legend values refer to t_{cool} or t_{dep} for a given data set, in units of τ_α (calculated at $T = 1.10\,T_g$ Supplementary Fig. 3). The ideal substrate temperature decreases as t_{dep} increases for PVD films (Supplementary Table 1). Error bars represent 95 % confidence intervals. (b) Inherent structure energies of liquid-cooled films at $T = 0.25\,T_g$ vs t_{cool} with power law fit from Equation 1. Colors of the points correspond to the same cooling or deposition rates as in (a). If a point is grey, that particular cooling rate is not shown in panel (a). 95% confidence intervals are shown. The X's represent predicted t_{cool} values necessary to form liquid-cooled films with energy equal to PVD films, as calculated using Equation 1. PVD film energies in panel (b) correspond to that of the substrate temperature that yields optimal stability for each t_{dep}.

As PVD films are formed more slowly, the inherent structure energy apparently approaches that of the deepest minima in the amorphous region of the potential energy landscape. By setting the liquid cooling time equal to infinity in Equation 1, one can estimate that these lowest energy states have inherent structure energies of -3.98. By this prediction, the most stable configurations produced here for $t_{dep} = 1.4 \times 10^4$ with $T_s = 0.67\,T_g$ are only 0.013 above this value. We emphasize here that these estimates should be viewed with some skepticism, as the curve shown in the inset of Figure 3 extends well beyond the data that can be generated with available computational resources. Also note that the more stable vapor deposited films show a similar, slowing rate of change for inherent structure energy as a function of deposition time, which we believe supports the idea that these films are gradually approaching the bottom of the amorphous regions of the potential energy landscape.

While the overall composition of each film is fixed, the local composition of the bulk region cannot be controlled precisely. On average, type A particles are excluded from the bulk, and the degree of exclusion varies by film formation type and formation time. It has been shown that E_{IS} for 3D $Ni_{80}P_{20}$ films depends linearly on composition over a small range [26]. That linear dependence is also observed in our 2D films. To account for the variation in E_{IS} due to composition effects, we perform linear fits of E_{IS} to χ_A for several cooling times. We find $\partial E_{IS}/\partial \chi_A = 1.6$ near $\chi_A = 0.65$ fits well across a wide range of film formation times during both liquid cooling and vapor deposition. The energy of all films is thus interpolated to $\chi_A = 0.65$ for all films, including those used in Figure 3. The average χ_A values for PVD and liquid-cooled films in the bulk are 0.648 and 0.637, respectively.

While the aim of this work is to investigate how vapor deposition may influence the structure of glass films, it is worth pointing out that for situations where PVD films and liquid-cooled films exhibit comparable structures, vapor deposition provides an efficient computational method for generating low-energy glasses. For instance, forming a liquid-cooled film with $t_{cool} = 1.4 \times 10^5\,\tau_\alpha$ requires 5.0×10^7 time units and 5.0×10^5 seconds on a particular machine. To form a vapor deposited film of equal energy, one can deposit with $t_{dep} = 1.4 \times 10^2 \tau_\alpha$ and $T_s = 0.76\,T_g$, which requires 5.12×10^6 time units and 4.1×10^4 seconds on the same machine, or approximately one order of magnitude less CPU time. Using predicted equivalent cooling rates from Table 1 in the Supplementary Information, we anticipate that this difference becomes greater for more stable, lower-energy films. We estimate that our most stable PVD films, prepared with $t_{dep} = 1.4 \times 10^4\,\tau_\alpha$, would require over three orders of magnitude more CPU time if prepared by liquid cooling.

Kinetic properties

The stability of the PVD films prepared here, based upon two measures, is comparable to that observed in experiment. First, we calculate the fictive temperature, T_f, of several liquid-cooled and PVD films. The fictive temperature is defined as the temperature at which the energy line extrapolated from the glass phase meets the energy line extrapolated from the equilibrium liquid phase, as shown in Figure 4. In the experiments of Swallen et al., the fictive temperature of the glass former 1,3-bis-(1-naphthyl)-5-(2-naphthyl)benzene (TNB) ($T_g = 347\ K$) was measured for three types of films: ordinary liquid-cooled films, aged liquid-cooled films, and PVD films[3]. These authors found the T_f of these films to be $0.99\,T_g$, $0.95\,T_g$, and $0.91\,T_g$, respectively. Later work in which PVD films were formed at slower deposition rates yielded TNB films with T_f of $0.88\ T_g$ [27]. Following their work, we calculate T_f for three types of films: films formed by liquid-cooling with $t_{cool} = 1.4 \times 10^1\ \tau_\alpha$, films formed by liquid-cooling with $t_{cool} = 1.4 \times 10^6\ \tau_\alpha$ (analogous to an aged glass prepared by liquid cooling), and films formed by vapor deposition using our slowest deposition rate, $t_{dep} = 1.4 \times 10^4\ \tau_\alpha$. The results are shown in Figure 4. We find $T_f = 1.05\ T_g$, $0.94\ T_g$ and $0.89\ T_g$ for the three classes of films, respectively. To measure T_f, films were heated at a constant rate of 2×10^{-6} from well below T_g. The ordering and spread of the corresponding fictive temperatures from simulations are consistent with those found in experiment.

Second, we calculate transformation times for both liquid-cooled and PVD films and compare them to experiment. The transformation time is defined as the time required for a material to melt after rapid heating to a temperature above T_g. Ultrastable PVD glasses have been shown to melt through a liquid front that originates at the surface of the film. Growth front velocities for ultrastable indomethacin (IMC) have been measured across a wide range of temperatures above T_g. These velocities have been found to be constant over a wide range of film thicknesses [28]. We measure film transformation times by rapidly heating films from below T_g to $1.1\ T_g$, and determining the time required for the film to

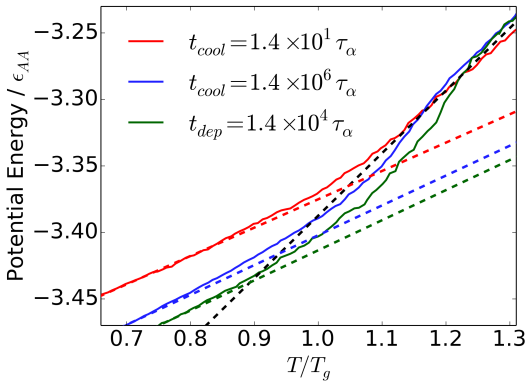

Figure 4: Potential energy versus temperature for PVD and liquid-cooled films on heating. Fictive temperatures, T_f, are calculated for three types of films: Shown in red and blue are films formed by liquid cooling at our smallest and largest cooling time, respectively. Shown in green are films formed by vapor deposition at our largest deposition time. The fictive temperatue is calculated to be the temperature where the extrapolated liquid line (dashed black) meets the extrapolated glass lines (dashed red, blue, green). Films are heated from below T_g at a constant rate of 2×10^{-6} in reduced units. We calculate fictive temperatures of 1.05 T_g and 0.94 T_g for the liquid cool films, and 0.89 T_g for the PVD films.

reach an equilibrium energy, as described in the Methods section. The results, normalized by τ_α at $T = 1.1\ T_g$, are shown in Figure 4 in the Supplementary Information. Energies used to calculate these transformation times are shown in Figure 5 of the Supplementary Information. The experimental τ_α of IMC at $T = 1.1\ T_g$ is 1.3×10^{-4} seconds, while our 2D system shows a τ_α of 1.48×10^{-10} seconds assuming a Ni-P model. Our most stable PVD films show a transformation time of 158 τ_α, and are 8.93 nm thick, using a Ni-P model. Using data from the literature, we calculate that a 8.93 nm thick film of IMC would melt over 354 τ_α, where τ_α is measured at 1.1 T_g for IMC[28]. By this comparison, our PVD films are just over half as stable as would be expected experimentally for films of this thickness. Note, however, that this comparison is highly speculative, given that both the materials and dimensionality of these two types of films are different. We suggest that the lower stability observed in simulations relative to experiment is expected, given that our slowest film growth rate (using a Ni-P model) is 48 μm per second. Experimental growth rates are typically a few nanometers per second, i.e. several orders of magnitude slower. Additional details on the conversion to real units and film growth rates are given in the Methods.

Comparison with 3D films

Vapor deposition in two dimensions is more efficient than in three dimensions. Two-dimensional films exhibit surface regions which show higher mobility than 3D films assembled using comparable models. This trait allows 2D materials to explore configuration space more effectively, which we suggest leads to the lower inherent structure energy seen in 2D. To compare 2D and 3D films formed by PVD, we examine 3D films with the same interaction parameters as in 2D, but with $\chi_A = 0.80$, as in previous work [26, 11]. We define the efficiency of vapor deposition as the ratio of a PVD film's growth rate to the film's equivalent liquid cooling rate. In 2D, equivalent t_{cool} values are found using the power law shown in Equation 1. In 3D, E_{IS} is linearly fit to $\log(t_{cool})$ for accessible cooling rates. By combining results from 3D films generated using NVE deposition (Supplementary Fig. 6) with the 2D data presented here, we estimate that vapor deposition in 2D is between 6×10^1 and 6×10^2 times more efficient than in 3D for the films with the lowest inherent structure energies.

Molecules near the surface of a glassy film are more mobile than those in the bulk [30]. Highly mobile molecules can explore configurations more rapidly, thereby allowing films prepared by vapor deposition to reach lower energies than those without mobile surface regions. Consistent with this understanding of surface mobility and our estimated efficiencies, we find that molecules near the surface of 2D films are both more mobile and encompass a thicker region than in 3D. To quantify these observations, we calculate $\langle \Delta r^2 \rangle$ of 2D and 3D films for a range of temperatures and film stabilities. For 2D and 3D samples held

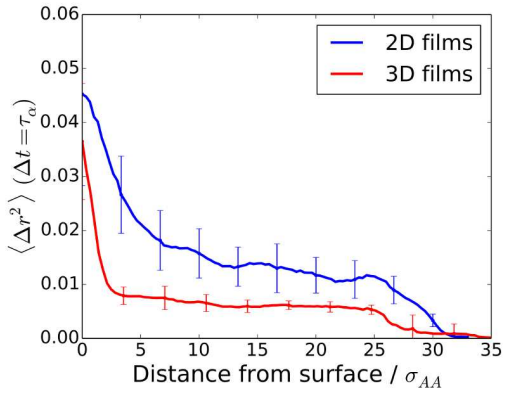

Figure 5: Mobility of atoms in both 2D and 3D PVD films. We measure $\langle \Delta r^2 \rangle$ with respect to distance from film surface calculated over $\tau_{\alpha,2D}$ time units for 2D and 3D films. Both films were formed with $t_{dep} = 1.4 \times 10^1 \, \tau_{\alpha,2D}$, which gives nearly equal film growth rates. The films are held at $T = 0.75 \, T_g$. Comparing 2D to 3D, the surface region is 70% more mobile and nearly twice as thick in 2D. The surface region is defined using the distance from surface where linear interpolations of the bulk region and the more steeply sloped surface region meet. Error bars represent the standard error from 20 2D and 3D films.

at $T = 0.75 \, T_g$, we find that molecules in the surface region are, on average, 70% more mobile than those in the bulk. The high-mobility region extends nearly twice as far into the film than in 3D, as shown in Figure 5. Surface mobilities do not depend strongly on film stability (Supplementary Fig. 7), though mobilities do depend on film temperature (Supplementary Fig. 8) and particle type (Supplementary Figs. 9, 10). Mechanistically, we suggest that the thicker and more mobile surface layer in 2D allows atoms to sample more configurations before being frozen into their glassy states, thereby enabling exploration of lower energy basins along the free energy landscape.

Heat transfer through films

As hot vapor particles impact the surface of growing films, energy is transferred from the vapor into the film. In this material, heat transfers along tightly coupled strings of particles. Correlated strings of particles in glasses have been reported before[31]. Note, however, that the strings discussed here are inherently different as they correspond to events initiated by newly deposited hot surface particles that introduce a disturbance. Several representative configurations of long strings are shown in Figure 6. Particles in these thin strings reach kinetic energies near that of the vapor particle at impact. While 75% of these strings penetrate less than 4 atom diameters into the film, occasionally, such strings can be significantly longer. In 3% of the cases, strings penetrate over seven atom diameters into the film, thereby providing a highly focused energy transfer process down to a relatively large depth.

Heat transferred along strings enters the film much more rapidly than would be expected from a diffusive mechanism. To illustrate the difference, one can rely on a simple one-dimensional continuum model where heat only transfers by diffusion. The continuum model's surface is initialized at a high temperature, such that the total amount of heat added to the continuum and molecular dynamics models are the same. Parameters for the continuum model, such as heat capacity and thermal diffusivity, are determined from molecular dynamics simulations as described in the Methods section. One can then generate temperature profiles with respect to distance from the film's surface of these two models as they evolve in time. Figure 7 shows the temperature profile of the PVD films shown in Figure 6 as compared to the continuum model at $1.1 \times 10^{-2} \tau_\alpha$ after impact or initialization. If one looks at heat transfer averaged over many films, the continuum results are recovered (Supplementary Fig. 11). However, in the case of long strings, heat transfer is much faster and energy is much more localized than in the continuum case, as shown in Figure 7.

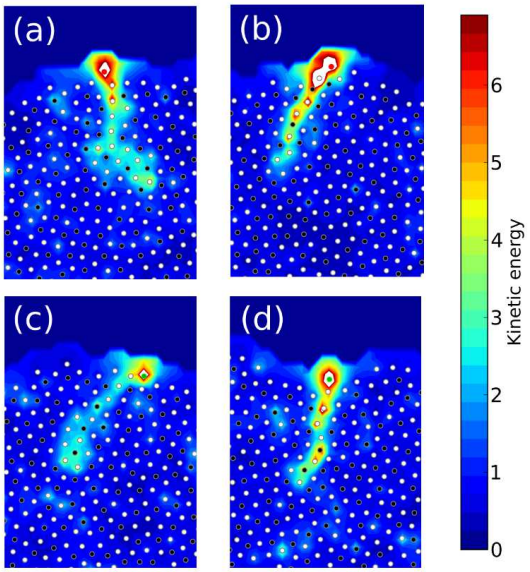

Figure 6: Strings of high-energy particles resulting from the impact of a vapor atom during the PVD process. The four panels, (a), (b), (c), and (d), show independent examples of energy transfer along strings of particles after a vapor particle impacts the surface of the film. The kinetic energy of each particle is normalized by $k_B T_g$. Prior to impact, the films were equilibrated at $T = 0.5\,T_g$. As energy travels through the string, it is localized to only one or two atoms at a time. For clarity, atoms involved in a string are shown with their maximum kinetic energy over the lifetime of the string. The particle that impacted the surface is colored red or green, depending on whether it is of type A or B, respectively. Particles already in the film are colored white or black for type A or B, respectively.

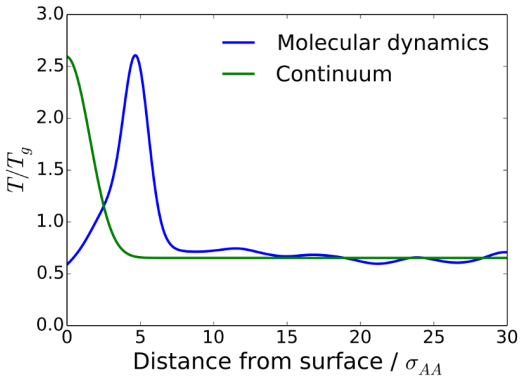

Figure 7: Temperature profiles resulting from continuum and molecular dynamics heat transfer when vapor particle impacts on the surface of a film. The temperature profile of molecular dynamics simulations shown in Figure 6 is shown $2.6 \times 10^{-4} \tau_\alpha$ after the impact of a vapor atom, as compared to temperature profile from similar continuum simulation. The continuum simulation is initialized with a high temperature at its surface to match heat added by vapor atoms' impact. Molecular dynamics simulations which show long strings are used to show the process's effect on thermal transport. The molecular dynamics temperature profile is taken from a narrow slice of the film around the four strings shown in Figures 6, such that the temperature increase can be easily resolved.

Structural features

The 2D films considered here exhibit considerable local pentagonal and rectangular order. Figures 1 and 10 show representative configurations of the system. The q_5 and q_8 order parameters (which select for local pentagonal and rectangular order, respectively), are used here to analyze the structure of the films[21]. Additional details on the order parameters' selectivity for different geometries are given in Figues 12-14 of the Supplementary Information. The q_l order parameter, which is calculated for each particle based on the arrangement of its neighbors, is defined in Equation 2, where a is a particle, N is the set of a's neighbors, and Y_{lm} is the spherical harmonic for the specified l and m:

$$q_l(a) = \sqrt{\frac{4\pi}{2l+1} \sum_{m=-l}^{m \leq l} |q_{lm}(a)|^2} \tag{2}$$

$$q_{lm}(a) = \frac{1}{\widetilde{N}} \sum_{n \in N} Y_{lm}(a \rightarrow n) \tag{3}$$

High q_5 pentagons tend to form mostly as five white type A particles surrounding a single black type B particle. For this reason, q_5 is calculated only for type B particles. The q_8 parameter is calculated for all atoms. The nearest four neighbors of atoms in high q_8 rectangular structures tend to be of different type, thereby maximizing the A-B interaction. Figure 1 shows a contour map of $\overline{q_5}$ and $\overline{q_8}$ values calculated for a liquid-cooled film with a cooling time of $t_{cool} = 1.4 \times 10^1$. Here $\overline{q_l}$ denotes a time averaged q_l parameter averages over in-cage vibrations, as defined in Equation 5 in Methods. It can be seen that high-q_8 clusters are of medium size, while locally-ordered q_5 clusters, which cannot tessellate, appear to be pentagonal. A similar coexistence of medium-range ordered clusters and locally-ordered structures was reported in a simulated atomic glass system in which particles' anisotropy frustrated crystallization[32].

To assess the extent of order in these films, particle groups are classified as highly ordered or not using a simple cutoff scheme described in Methods. High-order cutoff values are chosen to be $\phi_5 = 0.55$ and $\phi_8 = 22.0$, or 78% and 34% of their values relative to perfectly pentagonal or square configurations (which yield the maximum values for these order parameters). All results can be reproduced using different cutoffs as shown in Figures 15-20 of Supplementary Information.

We define the degree of order, D_l, as the fraction of particles involved in high-l ordered groups. We plot the D_l for all PVD and liquid-cooled films in Figure 8. We find that as the films become more stable, the q_8 character decreases, while the q_5 character increases. This can be appreciated by visually comparing Figure 8 to Figure 3, and by comparing the relatively unstable film in Figure 1 to the relatively stable films in Figure 10. Given the direct relationship between these parameters and E_{IS}, we conclude that the structure and stability of these films are well captured by the q_5 and q_8 parameters.

Figure 9 shows the degree of q_5 and q_8 order vs. E_{IS} for all liquid-cooled and PVD films. Only data from films well in the glassy state, $T < 0.2$, are included. The q_5 and q_8 trends with temperature are similar and independent of the process of formation. These results can in fact be used to estimate inherent structure energy from degree of order since both D_5 and D_8 behave monotonically with E_{IS}. The degree of q_8 order for PVD films on average lies slightly below that of liquid-cooled films. We attribute this slight difference to the differences in composition between PVD and liquid-cooled films: on average, their bulk compositions are $\overline{\chi_A} = 0.648, 0.637$, respectively.

Note, however, that more subtle differences could in principle exist between PVD and liquid-cooled samples. Figure 10 compares vapor deposited and liquid samples with $E_{IS} \approx -3.95$. The contour map shows no systematic differences in high-order cluster size, location, or shape. We find that the size of high-order clusters dependly only on E_{IS} as well, not formation method (Supplementary Fig. 21). Radial distribution functions and structure factors are also calculated for liquid-cooled and PVD films of equal energy, and we find no systemic differences between the two (Supplementary Figs. 22-29). Comparing the film in Figure 1 to the more stable films in Figure 10, one can appreciate the increase in q_5 and the corresponding decrease in q_8 character that comes with increasing stability.

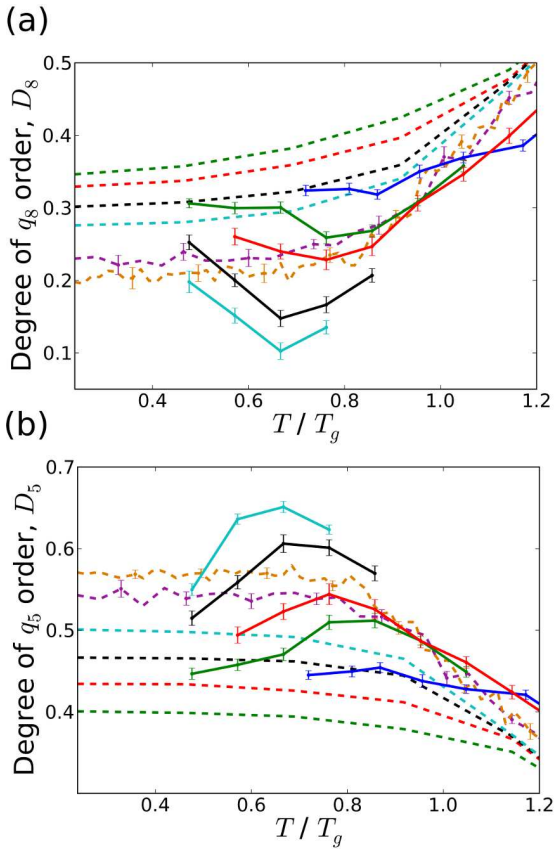

Figure 8: Degree of q_5 and q_8 order in PVD and liquid-cooled films. Dashed lines represent data from liquid-cooled films, while solid lines represent data from PVD films. Panel (a) shows data for the q_8 order parameter while Panel (b) shows data for the q_5 order parameter. The colors correspond to the same rates as in Figure 3, where blue is $t = 1.4 \times 10^0\ \tau_\alpha$, orange is $t = 1.4 \times 10^6\ \tau_\alpha$, and colors in between are separated by one order of magnitude in cooling rate. D_5 increases with film stability while D_8 decreases. These data show the same trends as the inherent structure energy shown in Figure 3, suggesting that these metrics provide a quantitative link between structure and stability in these glassy films. D_8 is calculated using all particles in the bulk, while D_5 is calculated using only type B particles in the bulk, as pentagonal structures form almost exclusively around these atoms. Error bars represent the standard error; they are only shown for liquid-cooled samples when the error is non-negligible.

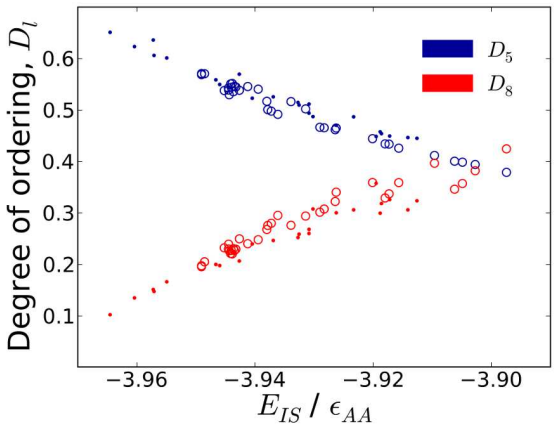

Figure 9: Degree of q_5 and q_8 ordering for vapor deposited and liquid-cooled films versus inherent structural energy. Solid circles represent vapor deposited data while open circles represent liquid-cooled data. Data for liquid cooling is taken from runs with t_{cool} ranging from $1.4 \times 10^1\,\tau_\alpha$ and $1.4 \times 10^6\,\tau_\alpha$, while data for vapor deposition is taken from runs with t_{dep} ranging from $1.4 \times 10^0\,\tau_\alpha$ to $1.4 \times 10^4\,\tau_\alpha$. Only data from films with $T < 0.5T_g$ are used. q_5 and q_8 show an inverse relationship with q_5 increasing with film stability and q_8 decreasing. The q_l values of films with equal energy appear substantially equivalent regardless of film formation style, considering that compositions of the two types of films are not identical.

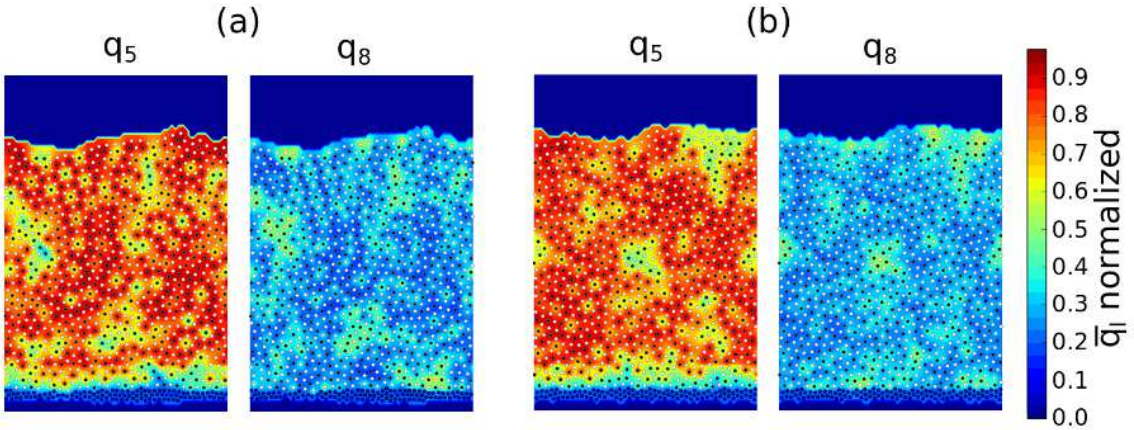

Figure 10: Contour maps of q_5 and q_8 for liquid-cooled and PVD films both with $E_{IS} = -3.95$. Panel (a) shows liquid-cooled film formed with $t_{cool} = 1.4 \times 10^5\,\tau_\alpha$ at $T = 0.25\,T_g$. Panel (b) shows vapor deposited film formed with $t_{dep} = 1.4 \times 10^3\,\tau_\alpha$ and $T_s = 0.75\,T_g$. These films are of equal inherent structural energy, allowing for direct comparison of the structures. The ordering within these two films shows no systemic differences, suggesting that isotropic PVD glasses are equilvalent to those formed by liquid cooling when the films are of equal inherent structure energy.

To conclude, a new method was introduced to prepare glasses in silico through a process of vapor deposition. The method was applied to investigate a model 2D glass forming liquid. After comparing the structure and energy of the resulting materials to that of ordinary liquid-cooled glassy films, it was found that *in-silico* physical vapor deposition greatly expands the range of film properties and structures that can be accessed as compared to traditional liquid cooling. In the 2D materials studied here, the range of structures includes pentagonal clusters and square-grid ordered regions of varying size. Under appropriate conditions, forming films by physical vapor deposition creates extremely low energy films, equivalent to liquid-cooled films cooled five orders of magnitude slower than possible on available computers. By varying the rate of vapor deposition, it is found that the ideal substrate temperature decreases with slowing deposition rate. In 2D, the surface layer of glassy films is thicker than it is in 3D, leading to a more effective PVD formation mechanism. Upon impacting a growing PVD film, newly deposited molecules form strings of hot particles that can reach well into the interior of the film, possibly providing an additional relaxation mechanism that helps the system explore its energy free landscape. An analysis using bond order parameters that select for square and pentagonal order revealed that films transition from a high square-grid character structure to a locally-ordered pentagonal structure as films stabilize. By examining the change in D_5 and D_8 in films formed using both methods, it was possible to establish that the degree of order does not depend on the formation type. More generally, the results presented in this work serve to demonstrate that, for the simple, isotropic model considered here, the glassy materials prepared by PVD are the same as those prepared by gradual cooling from the liquid phase, and that PVD glasses correspond to liquid-cooled glasses prepared at extremely slow cooling rates.

Methods

Simulation Parameters

The films in this work consist of a binary mixture of Lennard-Jones particles with a third particle type acting as the substrate. The interaction potential is given by Equation 4, where r is the distance between two particles, r_c is the distance beyond which interactions are not considered, and ϵ and σ change the strength and range of the interactions.

$$E = 4\epsilon\left((\frac{\sigma}{r})^{12} - (\frac{\sigma}{r})^{6}\right) \qquad r < r_c \tag{4}$$

These simulations use the values $r_c = 2.5$, $\epsilon_{AA} = 1.0$, $\epsilon_{AB} = 1.5$, $\epsilon_{BB} = 0.5$, $\sigma_{AA} = 1.0$, $\sigma_{AB} = 0.8$, $\sigma_{BB} = 0.88$. Values of ϵ and σ for the A and B particles acting on the substrate are 1.0 and 0.75, respectively. The masses of all particles are set to 1.0. The simulation box uses periodic boundary conditions in the x dimension and finite in y. The x dimension is parallel to the substrate while the y dimension is perpendicular. The simulations box is $30\sigma_{AA}$ wide and the height is set so that the boundary is $10\sigma_{AA}$ above the surface of the film as it grows. A timestep of $\Delta t = 0.005$ is used for all simulations. A Nosé-Hoover thermostat is used to maintain the temperature of all NVT ensembles [33].

Inherent structural energies were calculated by minimizing configurations using the FIRE algorithm with energy and force tolerances of 1×10^{-10}[34]. All simulations were performed using LAMMPS[35] and all figures were generated using Matplotlib[36].

Formation of PVD Films

Vapor deposited films are formed by initializing a substrate, then adding groups of atoms to the simulation box and allowing them to settle and cool on the growing film. The substrate is formed such that it does not impose any strong ordering the on film. First, substrate particles are randomly placed in a small rectangular area near the bottom of the simulation box. The rectangle spans the width of the box and is 3 σ_{AA} tall. The atoms are tethered to their original positions using harmonic springs with a spring constant $k = 5$. The substrate is then minimized using the FIRE algorithm. The substrate atoms are then re-tethered to their minimized positions using harmonic springs with $k = 1000$. The initial weak spring ensures that the substrate thickness stays roughly constant during the minimization. Throughout the simulation the temperature of the substrate is held constant using a Nosé-Hoover thermostat in an NVT ensemble as described above. A wall with a harmonic repulsive potential is placed 10 σ_{AA} above the substrate. The wall is moved as the film grows to keep the distance between the film and the wall constant.

The film is grown using the following method: Ten particles are initialized in a region $3-5\ \sigma_{AA}$ above the growing film. The particle types are chosen to keep the film configuration as close to $\chi_a = 0.65$ as possible. The particles are initialized with random velocities at $T = 1.0$, as in previous work[11, 26]. The new particles and the growing film are then simulated as an NVE ensemble for t_{dep}. The new particles cool by natural heat transfer through the growing film to the substrate. This process is repeated until the films have a height of approximately $35\sigma_{AA}$. Our method differs from previous work, where the film and vapor atoms are explicitly thermostatted. We find that this method produces lower energies than that employed in previous work (Supplementary Fig. 30) and that film temperature is well thermostatted by the substate (Supplementary Fig. 31).

In all but films formed with $t_{dep} = 1.4 \times 10^0$, the film temperature was tightly distributed around T_s. Film temperatures for those formed with $t_{dep} = 1.4 \times 10^0$ were deposited quickly enough that T_{film} was roughly $0.1\,T_g$ higher than T_s. In these cases, the actual temperature of the film was used in data.

Formation of Liquid Cooled Films

Liquid-cooled films are generated by heating vapor deposited films to $T = 1.0$, then recooling linearly over the time t_{cool}. The wall and substrate spring parameters are not changed during this process. To ensure the independence of each liquid-cooled film, the heated configurations are equilibrated for a random time ranging from 100 to 10000 time units while at $T = 1.0$. The films are cooled to $T = 0.05$, at which point the inherent structural energy has essentially stopped decreasing.

Transformation Time Measurements

Transformation times are measured by heating a film to $T = 1.1\ T_g$ over 100 time units, then setting the thermostat to $T = 1.1\ T_g$ and measuring the potential energy of the film as it melts. When a film's potential energy is 90% of the way from its initial energy to its final energy, it is said to be transformed. We find that if the films are instantaneously heated from very low temperatures ($T = 0.25\ T_g$) to above T_g, the films expand extremely quickly, push off the static substrate, effectively 'jump'. For this reason, we introduce the initial heating step.

Thermal Conductivity Measurements

Parameters for the one-dimensional continuum heat transfer were taken from molecular dynamics simulations. In the model, the equation $\frac{dT}{dt}c_v = q = \kappa\nabla T$ is iterated, where T is temperature, t is time, c_v is heat capacity, and κ is thermal conductivity. c_v is determined by heating the systems around in the temperature of interest, and measuring the energy required. Thermal diffusivity is measured using the Green-Kubo relation which relates the auto-correlation of heat flux to thermal diffusivity.

Order Parameters

We assess the order of the systems using a simple high-order cutoff. High-order cutoff values are chosen to be $\phi_5 = 0.55$ and $\phi_8 = 22.0$, or 78% and 34% of their values relative to perfectly pentagonal or square configurations. These cutoff values are chosen in order to discriminate between ordered and non-ordered configurations. Note, however, that the conclusions can be reproduced using other cutoffs (Supplementary Figs 15-20). To create an order metric independent of in-cage vibrations, we average the order parameter q_l defined in Equation 5 over τ_β. Here τ_β is taken to be 10 Lennard-Jones time units from the time at which the the self intermediate scattering function at $T = 0.8\ T_g$ has decayed to its in-cage plateau (Supplementary Fig. 32). This means that we are time averaging over the positions sampled within each atom's glassy cage.

$$\overline{q_l}(a,t) = \frac{1}{\tau_\beta}\int_{t-\frac{\tau_\beta}{2}}^{t+\frac{\tau_\beta}{2}} q_l(a(t'))dt' \tag{5}$$

Particles are then classified as transiently high-order if the $\overline{q}_l$ parameter is above the cutoff value as shown in Equation 6.

$$o_l(a,t) = \begin{cases} 1 & \bar{q}_l(a,t) \geq \phi_l \\ 0 & \bar{q}_l(a,t) < \phi_l \end{cases} \tag{6}$$

Finally, we label the particle as high-order if more than half of the transient high-order values in the averaging window of τ_β are 1. Since the q_8 metric is intended to select for larger-scale crystallinity, we mark high q_8 particles that appear in small clusters and thin strands as not highly ordered.

When selecting highly ordered q_8 clusters, two techniques are used to refine groupings. First, any cluster that is of 5 or fewer atoms is ignored. Second, we note that multiple q_8 clusters are occasionally connected by single-atom-wide chains of q_8-ordered atoms. For the purposes of counting cluster size, we would like to separate these clusters, as they are structurally distinct (but still connected). To do this, we remove particles from q_8 clusters using the following method: First, we count how many of a given atom's neighbors (within a radius of 1.2) are in a q_8 ordered group. Then we look at those ordered neighbor particles and perform the same count. If the sum of all of these ordered neighbors is less than five, we remove the particle from its ordered group, as the atom is likely part of some thin protrusion or connection. A neighbor cutoff of 1.2 was used for equation 3. This value represents the first minimum in the radial distribution function and gave good contrast for bond order parameter values.

Conversion to real units

In order to facilitate comparison to experiment, the Lennard-Jones units used in this work are converted to real units. We cast type A particles into nickel and type B particles into phosphorus. The simulated atom of nickel (type A) has mass and Lennard-Jones parameters of unity; to convert into real units, one only needs the energy, length, and mass by which those parameters were normalized. Dimensional analysis shows that the time unit in simulation is given by $t_{unit} = \sigma\sqrt{m/\epsilon}$, with Lennard-Jones parameters for nickel as $\epsilon = 5.65 kcal\ mol^{-1} = 23640 J\ mol^{-1}$, $\sigma = 2.552 \times 10^{-10} m$, and the mass is $58.69 \times 10^{-3} kg\ mol^{-1}$ [29]. Dividing the ϵ and mass by Avogadro's number, we find that the real time unit is 4.021×10^{-13} seconds. Our longest PVD simulations lasted 9.2×10^{10} simulation timesteps with $dt = 0.005$ Lennard-Jones time units, which translates into a real time of 1.85×10^{-4} seconds. Films are roughly 35 σ, or 8.93×10^{-9} meters thick, giving a growth rate of 48 μm per second.

References

[1] Angell, C. A. Formation of glasses from liquids and biopolymers. *Science* **267**, 1924–1935 (1995).

[2] Simon, S. L., Sobieski, J. W. & Plazek D. J. Volume and enthalpy recovery of polystyreme. *Polymer* **42**, 2555-2567 (2001).

[3] Swallen, S. F., Kearns, K., Mapes, M., Kim, Y., McMahon, R., Ediger, M. D., Wu, T., Yu, L. & bibinfoauthorSatija, S., Organic glasses with exceptional thermodynamic and kinetic stability. *Science* **315**, 353–356 (2007).

[4] Olsen, N. B., Dyre, J. C. & Christensen, T. Structural relaxation monitored by instantaneous shear modulus. *Phys. Rev. Lett.* **81**, 1031 (1998).

[5] Wang J. Q., Shen Y., Perepezko, J. H. & Ediger, M. D. Increasing the kinetic stability of bulk metallic glasses. *Acta Mater.* **104**, 25-32 (2016).

[6] Zhu, L. & Yu, L. Generality of forming stable organic glasses by vapor deposition. *Chem. Phys. Lett.* **499**, 62–65 (2010).

[7] Yu, L. Amorphous pharmaceutical solids: preparation, characterization and stabilization. *Adv. Drug Deliv. Rev.* **48**, 27–42 (2001).

[8] Kearns, K. L., Swallen, S. F., Ediger, M. D., Wu, T. & Yu, L. Influence of substrate temperature on the stability of glasses prepared by vapor deposition. *J. Chem. Phys.* **127**, 154702 (2007).

[9] Yang, Z., Fujii, Y., Lee, F. K., Lam, CH. & Tsui, O. KC. Glass transition dynamics and surface layer mobility in unentangled polystyrene films. *Science* **328**, 1676–1679 (2010).

[10] Zhu, L., Brian, CW., Swallen, S .F., Straus, P. T., Ediger, M. D. & Yu, L. Surface self-diffusion of an organic glass. *Phys. Rev. Lett.* **328**, 256103 (2011).

[11] Singh, S., Ediger, M. D. & de Pablo, J. J. Ultrastable glasses from in silico vapour deposition. *Nat. Mater.* **12**, 139-144 (2013).

[12] S. S. Dalal, D. M. Walters I. Lyubimov J. J. de Pablo & Ediger, M. D. Tunable molecular orientation and elevated thermal stability of vapor-deposited organic semiconductors. *Proc. Natl. Acad. Sci. USA* **112**, 4227–4232 (2015).

[13] Hocky, G. M., Berthier, L. & Reichman, D. R. Equilibrium ultrastable glasses produced by random pinning. *J. Chem. Phys.* **141**, 224503 (2014).

[14] Pieranski, P. Two-dimensional interfacial colloidal crystals. *Phys. Rev. Lett.* **45**, 569 (1980).

[15] Denkov, N., Velev, O., Kralchevski, P., Ivanov, I., Yoshimura, H. & Nagayama, K. Mechanism of formation of two-dimensional crystals from latex particles on substrates. *Langmuir* **8**, 3183–3190 (1992).

[16] Weeks, E., Crocker, J. C., Levitt, A., Schofield, A. & Weitz, D. A. Three-dimensional direct imaging of structural relaxation near the colloidal glass transition. *Science* **287**, 627–631 (2000).

[17] Ebert, F., Keim, P. & Maret, G. Local crystalline order in a 2D colloidal glass former. *EPJ E* **26**, 161–168 (2008).

[18] Lichtenstein, L., Büchner, C., Yang, B., Shaikhutdinov, S., Heyde, M., Sierka, M., Włodarczyk, R., Sauer, J. & Freund, H. The Atomic Structure of a Metal-Supported Vitreous Thin Silica Film. *Angew. Chem. Int. Ed.* **51**, 404–407 (2012).

[19] Huang, P. Y., Kurasch, S., Srivastava, A., Skakalova, V., Kotakoski, J., Krasheninnikov, A., Hovden, R., Mao, Q., Jannik, M., Smet, J., Muller, D. & Kaiser, U. Direct imaging of a two-dimensional silica glass on graphene. *Nano Lett.* **26**, 1081–1086 (2012).

[20] Zheng, Z., Wang, F. & Han, Y. Glass transitions in quasi-two-dimensional suspensions of colloidal ellipsoids. *Phys. Rev. Lett.* **107**, 065702 (2011).

[21] Steinhardt, P. J., Nelson, D. R. & Ronchetti, M. Bond-orientational order in liquids and glasses. *Phys. Rev. B.* **28**, 784 (1983).

[22] Shi, Z. Debenedetti, P. G. & Stillinger, F. H. Properties of model atomic free-standing thin films. *J. Chem. Phys.* **134** 114524 (2011).

[23] Debenedetti, P. G. & Stillinger, F. H. Supercooled liquids and the glass transition. *Nature* **410**, 259–267 (2001).

[24] Kearns, K. L., Swallen, S. F. & Ediger, M. D. Hiking down the Energy Landscape: Progress Toward the Kauzmann Temperature via Vapor Deposition. *J. Phys. Chem. B* **112**, 4934–4942 (2008).

[25] Yu, H.-B., Luo, Y. & Samwer, K. Ultrastable metallic glass. *Adv. Mater.* **25**, 5904–5908 (2013).

[26] Lyubimov, I., Ediger, M. D. & de Pablo, J. J. Model vapor-deposited glasses: Growth front and composition effects. *J. Chem. Phys.* **139**, 144505 (2013).

[27] Dawson, K., Zhu, L. Kopff, L. A. McMahon, R. J. Robert, J. Yu, L. & Ediger, M. D. Highly stable vapor-deposited glasses of four tris-naphthylbenzene isomers. *J. Phys. Chem. Lett.* **2**, 2683–2687 (2011).

[28] Rodríguez-Tinoco, C. Gonzalez-Silveira, M. Ràfols-Ribé, J. Lopeandía, A. Clavaguera-Mora, M. T. & Rodríguez-Viejo, J. Evaluation of Growth Front Velocity in Ultrastable Glasses of Indomethacin over a Wide Temperature Interval. *J. Phys. Chem. B* **118**, 10795–10801 (2014).

[29] Heinz, H. Vaia, R. A. Farmer, B. L. & Naik, R. R. Accurate simulation of surfaces and interfaces of face-centered cubic metals using 12- 6 and 9- 6 Lennard-Jones potentials. *J. Phys. Chem. C* **112**, 17281–17290 (2008).

[30] Brian, C. W. & Yu, L. Surface self-diffusion of organic glasses. *J. Phys. Chem. A* **117**, 13303–13309 (2013).

[31] Donati, C., Douglas, J., Kob, W., Plimpton, S., Poole, P. & Glotzer, S. Stringlike cooperative motion in a supercooled liquid. *Phys. Rev. Lett.* **80**, 2338 (1998).

[32] Shintani, H. & Tanaka, H. Frustration on the way to crystallization in glass. *Nature Phys.* **2**, 200–206 (2006).

[33] Martyna, G. J., Klein, M. L. & Tuckerman, M. Nosé–hoover chains: the canonical ensemble via continuous dynamics. *J. Chem. Phys.* **97**, 2635–2643 (1992).

[34] Bitzek, E., Koskinen, P., Gähler, F., Moseler, M. & Gumbsch, P. Structural relaxation made simple. *Phys. Rev. Lett.* **97**, 170201 (2006).

[35] Plimpton, S. Fast parallel algorithms for short-range molecular dynamics. *J. Comput. Phys.* **117**, 1–19 (1995).

[36] Hunter, J. D. Matplotlib: A 2d graphics environment. *Comput. Sci. Eng.* **9**, 90–95 (2007).

Acknowledgements

The authors would like to thank David Rodney for many useful conversations. This work was supported by a DMREF grant NSF-DMR-1234320. Fast GPU-accelerated codes for simulation of glassy materials were developed with support from DOE, Basic Energy Sciences, Materials Research Division, under MICCoM (Midwest Integrated Center for Computational Materials).

Author Contributions

Daniel Reid carried out the simulations. Daniel Reid, Ivan Lyubimov, Mark Ediger and Juan de Pablo analyzed and interpreted the results. Daniel Reid, Mark Ediger and Juan J. de Pablo concieved and planned the study and wrote the paper.

Competing financial interests

The authors declare no competing financial interests.